NASA TECHNICAL MEMORANDUM 89070

FINITE-ELEMENT ANALYSIS OF CORNER CRACKS IN RECTANGULAR BARS

I. S. Raju and J. C. Newman, Jr.

(NASA-TM-89070) FINITE-ELEMENT ANALYSIS OF CORNER CRACKS IN RECTANGULAR BARS (NASA) 47 p Avail: NTIS HC A03/MF A01 CSCL 20K

N87-25602

Unclas
G3/39 0083878

JUNE 1987

National Aeronautics and Space Administration

Langley Research Center
Hampton, Virginia 23665

FINITE ELEMENT ANALYSIS OF CORNER CRACKS IN RECTANGULAR BARS

I. S. Raju* and J. C. Newman, Jr.**
NASA Langley Research Center
Hampton, VA 23665-5225

SUMMARY

This paper presents stress-intensity factors for a wide range of quarter-elliptical corner cracks in rectangular bars. Cracked configurations were subjected to remote tension, in-plane bending, or out-of-plane bending. The ratio of crack depth to crack length ranged from 0.2 to 2; the ratio of crack depth to specimen thickness ranged from 0.2 to 0.8; and the ratio of crack length to specimen width ranged from 0.04 to 0.8. The configurations analyzed varied from a square bar to a very wide plate. These particular crack configurations were chosen to cover the range of shapes and sizes that have been observed to grow in experiments conducted on rectangular bars. The stress-intensity factors were calculated by a three-dimensional finite-element method. Finite-element models employed singularity elements along the crack front and linear-strain elements elsewhere. The models had about 7000 degrees of freedom. Stress-intensity factors were calculated using a nodal-force method.

The present results were compared with other numerical results for a quarter-circular corner crack configuration. The present results along the interior of the crack generally agreed within 3 percent with those from the literature. Some larger differences (3 to 13 percent) were observed near the intersection of the crack front and the free surfaces (in the

*Senior Scientist, Analytical Services & Materials, Inc., 107 Research Drive, Hampton, VA 23666. (work perfomed under contract NAS1-18256.)
**Senior Scientist, Materials Division.

boundary-layer region). Thus, analyses were also performed to study the effect of mesh refinement in the boundary-layer region and the influence of Poisson's ratio on the distribution of stress-intensity factors.

KEY WORDS: cracks, surface cracks, crack propagation, fracture, stress analysis, fatigue (materials), stress-intensity factors, finite elements, boundary-layer region

INTRODUCTION

Corner cracks can occur in many structural components. These cracks can cause premature failure of landing gear of aircraft, spars, stiffeners, and other reinforcements which employ rectangular-shaped components. Accurate stress analyses of these corner crack components are needed for reliable prediction of crack-growth rates and fracture strengths. An American Society for Testing and Materials (ASTM) Committee E24 Task Group has also proposed to include this crack configuration in E740 on Fracture Testing with Surface-Crack Tension Specimens.

One of the earliest analyses of a corner crack configuration was made by Tracey [1]. He analyzed a quarter circle corner crack in a quarter-circular bar subjected to remote tension using a three-dimensional (3-D) finite-element method. Tracey obtained the stress-intensity factor distribution for a shallow crack (ratio of crack depth to specimen radius was 0.2). Kobayashi and Enetanya [2] used the alternating method to obtain stress-intensity factors for corner cracks in three shapes (crack-depth-to-surface-half-length ratios of 0.98, 0.4, and 0.2). These results were obtained for uniform and

linearly varying crack-face pressure loadings. Pickard [3] used 3-D finite-element analyses to obtain stress-intensity factors for circular and elliptical cracks in rectangular bars for various values of crack-depth-to-specimen-thickness ratios. These results were obtained for uniform remote tensile loading. Newman and Raju [4,5] also used the 3-D finite-element method to obtain stress-intensity factors for corner cracks for a wide range of crack shapes and crack sizes in wide plates. They also presented empirical equations for stress-intensity factors obtained by curve fitting to the finite-element results and using engineering judgment. The results in references 4 and 5 were obtained for uniform tensile and out-of-plane bending loadings. While the results in references 4 and 5 are comprehensive, stress-intensity factor solutions are needed for a wide range in plate sizes (from a square bar to a wide plate). In addition to the two loadings used in references 4 and 5, the results for remote in-plane bending loading are also of interest.

This paper presents stress-intensity factors for a wide range of quarter-elliptical corner cracks in a rectangular bar as shown in figure 1. The bar was subjected to remote tension, in-plane bending, or out-of-plane bending loads. The ratio of crack depth to crack length (a/c) ranged from 0.2 to 2; the ratio of crack depth to specimen thickness (a/t) ranged from 0.2 to 0.8; and the ratio of crack length to specimen width (c/b) ranged from 0.04 to 0.8. The ratio of specimen width to thickness varied from a square bar to a very wide plate. Stress-intensity factors were calculated from a 3-D finite-element analysis using the nodal-force method [6-8]. The present results are compared with other numerical results from the literature for a shallow quarter-circular corner-crack configuration. Analyses were also

performed to study the effect of mesh refinement and the influence of Poisson's ratio on the distribution of stress-intensity factors in the boundary-layer region where the crack front intersects the free surface.

SYMBOLS

a	depth of corner crack
b	width of bar
c	length of corner crack
F	stress-intensity boundary-correction factor
h	half-length of bar
K	stress-intensity factor (mode I)
Q	shape factor for elliptical crack
S_{bx}	remote stress on outer fiber due to bending about x-axis (out-of-plane bending)
S_{bz}	remote stress on outer fiber due to bending about z-axis (in-plane bending)
S_t	remote uniform tensile stress
t	thickness of bar
x,y,z	Cartesian coordinate system
ν	Poisson's ratio
ϕ	parametric angle of ellipse

THREE-DIMENSIONAL FINITE-ELEMENT ANALYSIS

A three-dimensional finite-element analysis was used to calculate the mode I stress-intensity factor variations along the crack front for a corner crack in a bar, as shown in figure 1. In this analysis, Poisson's ratio (ν)

was assumed to be 0.3. In the investigation of the boundary-layer effect, however, Poisson's ratio was varied from 0 to 0.45.

Figure 2 shows a typical finite-element model for a corner crack in a rectangular bar. The finite-element models employed singularity elements along the crack front and eight-noded hexahedral elements elsewhere. The models had about 7000 degrees of freedom. Stress-intensity factors were evaluated using a nodal-force method. Details of the formulation of these types of elements, development of the models, and of the nodal-force method are given in references 6 through 8 and are not repeated here.

Loading

Three types of loads were applied to the finite-element models of the corner cracked bar: remote uniform tension, remote in-plane bending (bending about z-axis), and remote out-of-plane (bending about x-axis). The remote uniform tensile stress is S_t and the remote outer-fiber bending stresses are either S_{bx} or S_{bz}. The bending stress S_{bx} and S_{bz} are calculated at the origin of the surface crack ($x = y = z = 0$ in fig. 1) without the crack present.

Stress-Intensity Factor

The tensile and bending loads cause only mode I deformations. The mode I stress-intensity factor K for any point along the corner crack front was taken to be

$$K = S_i \left(\pi \frac{a}{Q}\right)^{1/2} F\left(\frac{a}{t}, \frac{a}{c}, \frac{c}{b}, \phi\right) \qquad (1)$$

where the subscript i denotes tension load ($i = t$) or bending loads

(i = bx or bz). The half-length of the bar, h, was chosen large enough to have a negligible effect on stress-intensity factors (h/b > 5). Values for F, the boundary-correction factor, were calculated along the crack front for various combinations of parameters (a/t, a/c, c/b, and ϕ). The crack dimensions and parametric angle, ϕ , are defined in figure 3. Note that the parametric angle is measured from the x-axis for all crack shapes. The shape factor for an ellipse, Q, is given by the square of the complete elliptic integral of the second kind.

The empirical expressions for Q (taken from ref. 7) used in this paper are

$$Q = 1 + 1.464(a/c)^{1.65} \quad \text{for } a/c < 1 \tag{2a}$$

$$Q = 1 + 1.464(c/a)^{1.65} \quad \text{for } a/c > 1 \tag{2b}$$

RESULTS AND DISCUSSION

The stress-intensity factors were obtained for corner cracks in bars subjected to the three loadings: remote uniform tension, out-of-plane bending, and in-plane bending. For these loading conditions, corner cracked bars with various crack sizes (a/t) and crack shapes (a/c) were analyzed. The range of the parameters considered were:

$a/t = 0.2, 0.5,$ and 0.8

$a/c = 0.2, 0.4, 1,$ and 2

$c/b = 0.04, 0.1, 0.2, 0.5,$ and 0.8

$h/b \geq 5$

For each of these combinations, stress-intensity factors were obtained along the crack front. Because of the voluminous results generated from this study, only typical results for each type of loading are shown. The complete

results are given Table 1. In all the figures, the normalized stress-intensity factor, $K/[S_i(\pi a/Q)^{1/2}]$, is presented as a function of the parametric angle, ϕ .

Rectangular Bar

Tensile loading.- Figure 4 presents the normalized stress-intensity factors for a quarter-circular corner crack (a/c = 1) in a large plate (c/b = 0.1). Because the crack shape is symmetric about $\phi = \pi/4$, the stress-intensity factors are also almost symmetric. The stress-intensity factors are slightly larger at $\phi = 0$ than at $\phi = \pi/2$. As expected, deeper cracks (larger a/t values) produced higher normalized stress-intensity factors.

Out-of-plane bending.- Figures 5 and 6 show the normalized stress-intensity factors for quarter elliptic corner cracks (a/c = 0.4 and 0.2, respectively) in a large plate (c/b = 0.1). At $\phi = 0$, deeper cracks gave higher normalized stress-intensity factors. However, at $\phi = \pi/2$, the stress-intensity factors are lower for deeper cracks. This behavior is expected because, at $\phi = \pi/2$, the crack front is in a lower stress field than that at $\phi = 0$. A comparison of figures 5 and 6 shows that the lower a/c ratio caused higher normalized stress-intensity factors at the maximum depth location ($\phi = \pi/2$) but caused lower normalized stress-intensity factors at the free surface ($\phi = 0$).

In-plane bending.- Figure 7 shows the normalized stress-intensity factors for a quarter-elliptic corner crack (a/c = 2) in a large plate (c/b = 0.1). Note that, in contrast to the earlier crack shapes, this crack shape has the major axis in the thickness direction. Figure 7 shows that

larger values of a/t produced larger normalized stress-intensity factors all along the crack front. There is no appreciable change in the shape of the stress-intensity factor distribution from shallow to deep cracks. Because of the large width (c/b = 0.1), under in-plane bending, the crack experiences a state of near uniform stress. Therefore, the stress-intensity factors for this case are not vastly different from those due to a remote tensile loading. Comparison of results from reference 4 with those in figure 7 confirms this observation.

Square Bar

As previously mentioned, the corner-crack specimen is being considered for inclusion in ASTM E740 on Fracture Testing of Surface-Crack Tension Specimens. One of the corner-crack configurations being considered is a square bar (b = t). Some typical results for a square bar with a quarter-circular corner crack (a/c = 1 and a/t = 0.2) subjected to all three loadings are presented in figure 8. In this figure the circular symbols denote the normalized stress-intensity factors due to remote tension, the square symbols denote the results due to out-of-plane bending, and the diamond symbols denote the results due to in-plane bending. As expected, the tensile loading produced higher normalized stress-intensity factors than the other loadings. Also, all the results are symmetric about $\phi = \pi/4$ because of the symmetric specimen configuration. Comparison of the results in figures 4 and 8 (c/b = 0.1 and 0.2, respectively) show that the normalized stress-intensity factors are larger for larger c/b. The results for the out-of-plane bending can be obtained from those for in-plane bending by changing ϕ to $\pi/2 - \phi$.

Comparison With Results From Literature

Figure 9 shows normalized stress-intensity factors calculated by several investigators for a quarter-circular corner crack in a rectangular bar ($a/t = 0.2$) subjected to remote tensile loading. The present finite-element results are shown as solid circular symbols and equation (27) of reference 4 is shown as the solid curve. Tracey [1] and Pickard [3] also used the finite-element method, but the width (b) and half length (h) of their model were equal to the thickness (see quarter-circular and square configurations in the insert in fig. 9). Kobayashi and Enetanya [2] used the alternating method. Their model had an a/c ratio of 0.98 and the width (b) and half length (h) were large compared to crack length. For all values of ν, Pickard's results were 1 to 3 percent higher than the present finite-element results. Part of the difference is due to a width and length effect in Pickard's model. Near $\phi = 0$ and $\pi/2$, Tracey's and Kobabyashi and Enetanya's results are 5 to 13 percent higher than the present results. All results are in good agreement (within 3 percent) at the midpoint ($\phi = \pi/4$).

Kobayashi and Enetanya's results [2] show a drop in the stress-intensity factor near the ends of the crack (at $\phi = 0$ and $\pi/2$). This is believed to be due to the boundary-layer effect at the locations where the crack front intersects a free surface [9-13]. The present finite-element model with eight wedges (fig. 2) did not show any boundary-layer effect. The boundary-layer effect is investigated in the next section by refining the finite-element model and by analyzing the configuration with several values of Poisson's ratio.

Boundary-Layer Effect on Stress-Intensity Factors

This section examines the boundary-layer effect where the crack front meets a free surface. To study this effect, a semi-circular surface crack ($a/c = 1$) in a large bar ($a/t = 0.2$ and $c/b = 0.04$) was used. The surface-crack configuration was chosen because, due to symmetry, only one of the locations where the crack meets the free surface needs to be analyzed. In contrast, the corner-crack configuration would require examination at two locations. However, the boundary-layer effect is expected to be identical for the two configurations.

Effect of mesh refinement.- Four different finite-element models with 8, 10, 14, and 16 wedges between $0 \le \phi \le \pi/2$ were considered. The 8-wedge model, shown in figure 2, has 8 equal wedges, each with a parametric angle of $\pi/16$. The other models have non-uniform wedges and were obtained by refining the 8-wedge model near the free surface. The smallest wedge angles for the 10-, 14-, and 16-wedge models are $\pi/64$, $\pi/128$, and $\pi/256$, respectively. The normalized stress-intensity factors for remote tensile loading obtained from these four models are shown in figure 10, where the parametric angle is measured from the free surface (see insert). Except for the 8-wedge model, the maximum stress-intensity factor occurred very near the free surface (at $\phi = \pi/80$ from the free edge). At the free edge, however, the stress-intensity factor dropped rapidly. The drop-off is most pronounced for the 16-wedge model. The stress-intensity factors in the interior ($\phi > \pi/80$) showed little or no change with mesh refinement. This strongly suggests that the region $0 \le \phi \le \pi/80$ is a boundary-layer region, where the computed stress-intensity factors depend on the mesh refinement and, hence, may not be reliable.

Although, as shown in figure 10, the stress-intensity factors show larger drop-offs at $\phi = 0$ with further mesh refinement, the peak values were nearly the same as that obtained from the 8-wedge model at $\phi = 0$ (within about 1.5 percent). Thus, the stress-intensity factors obtained from the 8-wedge model should be interpreted as an average value near the free surface. Results from the 8-wedge models at $\phi = 0$ have been successfully used to predict crack-growth patterns and lives for several surface- and corner-crack configurations and materials in reference 14.

Effect of Poisson's ratio.- Many investigators have postulated that the stress singularity where the crack front meets a free surface is different from the classical square-root singularity and is a function of Poisson's ratio (ν) of the material [9-13]. To study this, the 16-wedge model was analyzed with Poisson's ratios of 0, 0.3, and 0.45. (The limiting value of $\nu = .5$ was not analyzed because the three-dimensional finite-element analysis does not permit the use of this value.) Figure 11 presents the normalized stress-intensity factors obtained with these three Poisson ratios. For $\nu = 0$, the 16-wedge model does not show any drop-off in the stress-intensity factor at the free surface. But, higher values of Poisson's ratio showed large drop-offs near the free surface. References 9 through 13 showed that the power of the singularity has the largest deviation from the classical square root for $\nu = 0.5$. The present results appear to agree with these findings. Away from the free surface, higher Poisson's ratios gave higher stress-intensity factors (10 percent difference between results for Poisson's ratio of 0 and 0.45).

CONCLUDING REMARKS

Stress-intensity factors for corner cracks in rectangular bars have been obtained by a three-dimensional finite-element analysis. The bars were subjected to remote tension, out-of-plane bending, or in-plane bending loading. A wide range of crack shapes, crack sizes, and crack-length-to-specimen-width ratios were considered. Only typical results for each type of loading are presented in this paper.

For all loadings considered, smaller width bars produced higher normalized stress-intensity factors than the larger width bars. For tensile loading, quarter-circular corner cracks gave higher stress-intensity factors near the free surfaces and lower values in the interior. The maximum normalized stress-intensity factors occurred at the free surface along the width direction for cracks with crack-depth-to-length (a/c) ratios greater than 1 and at the free surface along the thickness direction for a/c less than 1.

For out-of-plane bending loading, the highest value of the normalized stress-intensity factor occurred at either end of a shallow crack (low crack-depth-to-specimen-thickness (a/t) ratios); the location depended on the crack shape. However, for deep cracks the highest values occurred at the free surface in the width direction. For bars of large widths, the normalized stress-intensity factors due to in-plane bending loading are nearly the same as those due to remote tension.

Stress-intensity factors from the present analysis for shallow quarter-circular corner cracks were compared to those in the literature for remote tensile loading. The present results for stress-intensity factors in the interior agreed well (within 3 percent) with those obtained by other three-

dimensional finite-element and alternating methods. Some differences (3 to 13 percent) were observed near the two free surfaces.

A boundary-layer effect exists at locations where a crack intersects a free surface. In the small region where the crack meets the free surface, the stress-intensity factors showed a sudden drop. The region in which this drop occurred has a parametric angle of about $\pi/80$ from the free surface. Smaller mesh refinements gave larger drop-offs. The boundary-layer effect is more pronounced for materials with larger Poisson ratios. Away from the free surface, higher Poisson ratios gave higher stress-intensity factors (10 percent difference between results for Poisson's ratio of 0 and 0.45).

The stress-intensity factors given in this paper should be useful in predicting crack growth rates and fracture strengths, in designing structural components and in establishing inspection intervals for structures subjected to cyclic loading.

REFERENCES

[1] Tracey, D. M., "3D Elastic Singularity Element for Evaluation of K Along an Arbitrary Crack Front," Int. J. of Fracture, Vol. 9, 1973, pp. 340-343.

[2] Kobayashi, A. S. and Enetanya, A. N., "Stress Intensity Factor of a Corner Crack," Mechanics of Crack Growth, ASTM STP-590, American Society for Testing and Materials, 1976, pp. 477-495.

[3] Pickard, A. C., "Stress-Intensity Factors for Cracks with Circular and Elliptic Crack Fronts - Determined by 3D Finite Element Methods," PNR-90035, Rolls-Royce Limited, May 1980.

[4] Newman, J. C., Jr. and Raju, I. S., "Stress-Intensity Factor Equations for Cracks in Three-Dimensional Finite Bodies," Fracture Mechanics: Fourteenth Symposium - Volume I: Theory and Analysis, ASTM STP-791, J. C. Lewis and G. Sines, Eds., American Society for Testing and Materials, 1983, pp. I-238 - I-265.

[5] Newman, J. C., Jr. and Raju, I. S., "Stress-Intensity Factor Equations for Cracks in Three-Dimensional Finite Bodies Subjected to Tension and Bending Loads," NASA TM-85793, April 1984.

[6] Raju, I. S. and Newman, J. C., Jr., "Three-Dimensional Finite-Element Analysis of Finite-Thickness Fracture Specimens," NASA TN D-8414, 1977.

[7] Raju, I. S. and Newman, J. C., Jr., "Improved Stress-Intensity Factors for Semi-Elliptical Surface Cracks in Finite-Thickness Plates," NASA TM X-72825, 1977.

[8] Raju, I. S. and Newman, J. C., Jr., "Stress-Intensity Factors for a Wide Range of Semi-Elliptical Surface Cracks in Finite-Thickness Plates," Engineering Fracture Mechanics, Vol. 11, No. 4, 1979, pp. 817-829.

[9] Hartranft, R. J. and Sih, G. C., "An Approximate Three-Dimensional Theory of Plates with Application to Crack Problems," Int. J. of Eng. Sci., Vol. 8, 1970, pp. 711-729.

[10] Benthem, J. P., "State of Stress at the Vertex of a Quarter-Infinite Crack in a Half-Space," Int. J. Solids and Structures, Vol. 13, 1977, pp. 479-492.

[11] Benthem, J. P., "The Quarter-Infinite Crack in a Half-Space: Alternative and Additional Solutions," Int. J. Solids and Structures, Vol. 16, 1980, pp. 119-130.

[12] Bazant, Z. P. and Estenssoro, L. F., "General Numerical Method for Three-Dimensional Singularities in Cracked or Notched Elastic Solids," Advances in Research on the Strength and Fracture of Materials, D. M. R. Taplin, Ed., Vol. 3a, Pergamon Press, 1977, pp. 371-385.

[13] Solecki, J. S. and Swedlow, J. L., "On the Three-Dimensional Implications of LEFM: Finite-Element Analysis of Straight and Curved Through Cracks in a Plate," ASTM STP-868, American Society for Testing and Materials, 1985, pp. 535-553.

[14] Newman, J. C., Jr. and Raju, I. S., "Prediction of Fatigue Crack-Growth Patterns and Lives in Three-Dimensional Cracked Bodies," Advances in Fracture Research, Proceedings of the 6th International Conference on Fracture (ICF6), New Delhi, India, December 4-10, 1984.

Table 1.- Stress-intensity factors for corner crack in a plate.

$a/c = 1.0$; $a/t = 0.2$; $h/b > 5$

$K/[S_i(\pi a/Q)^{1/2}]$

c/b	$2\phi/\pi$	TENSION	BENDING ABOUT X	BENDING ABOUT Z
0.04	0.000	1.1480	1.0543	1.0790
	0.125	1.1207	0.9956	1.0556
	0.25	1.0865	0.9214	1.0267
	0.375	1.0695	0.8655	1.0153
	0.50	1.0641	0.8234	1.0164
	0.625	1.0688	0.7953	1.0286
	0.75	1.0851	0.7833	1.0527
	0.875	1.1185	0.7894	1.0941
	1.000	1.1653	0.7944	1.1268
0.1	0.000	1.1542	1.0577	0.9926
	0.125	1.1268	1.0087	0.9726
	0.25	1.0923	0.9372	0.9503
	0.375	1.0752	0.8814	0.9471
	0.50	1.0697	0.8394	0.9581
	0.625	1.0745	0.8115	0.9814
	0.75	1.0909	0.8008	1.0176
	0.875	1.1246	0.8115	1.0709
	1.000	1.1516	0.8270	1.1107
0.2	0.000	1.1716	1.0807	0.8381
	0.125	1.1436	1.0264	0.8264
	0.25	1.1086	0.9527	0.8164
	0.375	1.0914	0.8964	0.8270
	0.50	1.0861	0.8544	0.8544
	0.625	1.0914	0.8270	0.8964
	0.75	1.1086	0.8164	0.9527
	0.875	1.1436	0.8264	1.0264
	1.000	1.1716	0.8381	1.0807

Table 1.- Continued.

$a/c = 1.0$; $a/t = 0.5$; $h/b > 5$

$K/[S_i(\pi a/Q)^{1/2}]$

c/b	$2\phi/\pi$	TENSION	BENDING ABOUT X	BENDING ABOUT Z
	0.000	1.2421	0.9863	1.1659
	0.125	1.2051	0.8849	1.1331
	0.25	1.1582	0.7479	1.0921
	0.375	1.1315	0.6313	1.0716
0.04	0.50	1.1197	0.5338	1.0666
	0.625	1.1216	0.4578	1.0760
	0.75	1.1383	0.4066	1.1004
	0.875	1.1747	0.3795	1.1444
	1.000	1.2041	0.3638	1.1792
	0.000	1.2612	0.9971	1.0938
	0.125	1.2232	0.9052	1.0637
	0.25	1.1750	0.7696	1.0287
	0.375	1.1473	0.6512	1.0159
0.1	0.50	1.1348	0.5523	1.0205
	0.625	1.1366	0.4756	1.0410
	0.75	1.1533	0.4242	1.0774
	0.875	1.1903	0.4017	1.1334
	1.000	1.2201	0.3977	1.1754
	0.000	1.3088	1.0329	0.9599
	0.125	1.2685	0.9349	0.9376
	0.25	1.2174	0.7959	0.9140
	0.375	1.1880	0.6763	0.9146
0.2	0.50	1.1749	0.5768	0.9356
	0.625	1.1770	0.5001	0.9749
	0.75	1.1953	0.4494	1.0319
	0.875	1.2350	0.4267	1.1095
	1.000	1.2671	0.4192	1.1669

	0.000	1.5469	1.1941	0.5898
	0.125	1.4920	1.0842	0.5856
	0.25	1.4231	0.9318	0.5922
	0.375	1.3856	0.8054	0.6325
0.5	0.50	1.3735	0.7047	0.7047
	0.625	1.3856	0.6325	0.8053
	0.75	1.4232	0.5922	0.9318
	0.875	1.4920	0.5856	1.0842
	1.000	1.5469	0.5898	1.1940

Table 1.- Continued.

$a/c = 1.0$; $a/t = 0.8$; $h/b > 5$

$K/[S_i(\pi a/Q)^{1/2}]$

c/b	$2\phi/\pi$	TENSION	BENDING ABOUT X	BENDING ABOUT Z
	0.000	1.4313	0.9714	1.3460
	0.125	1.3649	0.8151	1.2851
	0.25	1.2760	0.5984	1.2038
	0.375	1.2065	0.4057	1.1424
0.04	0.50	1.1856	0.2391	1.1286
	0.625	1.1825	0.1112	1.1337
	0.75	1.2257	0.0183	1.1835
	0.875	1.3008	-0.0370	1.2651
	1.000	1.3720	-0.0612	1.3404
	0.000	1.4696	0.9830	1.2877
	0.125	1.4001	0.8352	1.2283
	0.25	1.3069	0.6185	1.1519
	0.375	1.2338	0.4222	1.0979
0.1	0.50	1.2107	0.2533	1.0924
	0.625	1.2065	0.1242	1.1084
	0.75	1.2498	0.0309	1.1696
	0.875	1.3264	-0.0194	1.2630
	1.000	1.3992	-0.0319	1.3451
	0.000	1.5651	1.0310	1.1799
	0.125	1.4888	0.8747	1.1270
	0.25	1.3863	0.6521	1.0607
	0.375	1.3064	0.4527	1.0200
0.2	0.50	1.2802	0.2821	1.0294
	0.625	1.2758	0.1525	1.0656
	0.75	1.3228	0.0629	1.1474
	0.875	1.4064	0.0103	1.2640
	1.000	1.4856	-0.0056	1.3630

	0.000	2.075	1.2816	0.9423
	0.125	1.953	1.0998	0.8946
	0.25	1.794	0.8449	0.8477
	0.375	1.677	0.5233	0.8432
0.5	0.50	1.644	0.4434	0.9025
	0.625	1.658	0.3167	1.0136
	0.75	1.752	0.2407	1.1805
	0.875	1.911	0.2193	1.3989
	1.000	2.056	0.2282	1.5733
	0.000	3.1711	1.8318	0.6981
	0.125	2.8561	1.5519	0.6205
	0.25	2.5007	1.1950	0.5643
	0.375	2.2911	0.9190	0.5989
0.8	0.50	2.2325	0.7165	0.7164
	0.625	2.2911	0.5990	0.9188
	0.75	2.5007	0.5644	1.1968
	0.875	2.8561	0.6206	1.5516
	1.000	3.1711	0.6982	1.8315

Table 1.- Continued.

$a/c = 0.2$; $a/t = 0.2$; $h/b > 5$

$K/[S_i(\pi a/Q)^{1/2}]$

c/b	$2\phi/\pi$	TENSION	BENDING ABOUT X	BENDING ABOUT Z
	0.000	0.6157	0.5824	0.5710
	0.125	0.6480	0.5890	0.6018
	0.25	0.7483	0.6508	0.6979
	0.375	0.8650	0.7236	0.8123
0.04	0.50	0.9670	0.7802	0.9164
	0.625	1.0494	0.8211	1.0052
	0.75	1.1128	0.8503	1.0784
	0.875	1.1549	0.8669	1.1324
	1.000	1.1583	0.8571	1.1445
	0.000	0.6173	0.5805	0.5023
	0.125	0.6496	0.5850	0.5309
	0.25	0.7501	0.6471	0.6204
	0.375	0.8671	0.7197	0.7308
0.1	0.50	0.9693	0.7762	0.8373
	0.625	1.0519	0.8169	0.9351
	0.75	1.1155	0.8461	1.0226
	0.875	1.1577	0.8627	1.0939
	1.000	1.1611	0.8526	1.1189
	0.000	0.6208	0.5794	0.4007
	0.125	0.6534	0.5998	0.4256
	0.25	0.7544	0.6588	0.5065
	0.375	0.8721	0.7310	0.6129
0.2	0.50	0.9750	0.7876	0.7261
	0.625	1.0582	0.8288	0.8414
	0.75	1.1224	0.8584	0.9548
	0.875	1.1652	0.8762	1.0568
	1.000	1.1688	0.8696	1.1040

	0.000	0.6348	0.6082	0.0850
	0.125	0.6677	0.6169	0.1000
	0.25	0.7708	0.6813	0.1525
	0.375	0.8914	0.7575	0.2446
0.5	0.50	0.9976	0.8174	0.3754
	0.625	1.0846	0.8615	0.5412
	0.75	1.1530	0.8945	0.7308
	0.875	1.2003	0.9162	0.9246
	1.000	1.2066	0.9100	1.0392

Table 1.- Continued.

$a/c = 0.2$; $a/t = 0.5$; $h/b > 5$

$K/[S_i(\pi a/Q)^{1/2}]$

c/b	$2\phi/\pi$	TENSION	BENDING ABOUT X	BENDING ABOUT Z
	0.000	0.7905	0.6602	0.7386
	0.125	0.8179	0.6271	0.7648
	0.25	0.9348	0.6449	0.8770
	0.375	1.0796	0.6737	1.0187
0.04	0.50	1.2112	0.6855	1.1517
	0.625	1.3251	0.6869	1.2715
	0.75	1.4196	0.6876	1.3757
	0.875	1.4960	0.6934	1.4640
	1.000	1.5232	0.6848	1.4996
	0.000	0.7991	0.6637	0.6670
	0.125	0.8264	0.6288	0.6911
	0.25	0.9439	0.6474	0.7964
	0.375	1.0896	0.6768	0.9336
0.1	0.50	1.2219	0.6891	1.0687
	0.625	1.3365	0.6910	1.1973
	0.75	1.4316	0.6921	1.3157
	0.875	1.5085	0.6981	1.4210
	1.000	1.5359	0.6894	1.4696
	0.000	0.8199	0.6832	0.5631
	0.125	0.8464	0.6331	0.5846
	0.25	0.9657	0.6566	0.6805
	0.375	1.1139	0.6888	0.8131
0.2	0.50	1.2485	0.7032	0.9543
	0.625	1.3654	0.7068	1.1002
	0.75	1.4628	0.7096	1.2448
	0.875	1.5421	0.7167	1.3817
	1.000	1.5706	0.7059	1.6529

	0.000	0.8913	0.7297	0.2370
	0.125	0.9163	0.6972	0.2477
	0.25	1.0414	0.7191	0.3148
	0.375	1.1999	0.7556	0.4324
0.5	0.50	1.3465	0.7759	0.5926
	0.625	1.4778	0.7872	0.7922
	0.75	1.5925	0.7997	1.0195
	0.875	1.6916	0.8193	1.2565
	1.000	1.7322	0.8195	1.4001
	0.000	1.0030	0.8179	-0.1235
	0.125	1.0180	0.7762	-0.1240
	0.25	1.1444	0.7983	-0.0889
	0.375	1.3110	0.8387	0.0117
0.8	0.50	1.4689	0.8638	0.1905
	0.625	1.6162	0.8828	0.4441
	0.75	1.7535	0.9074	0.7546
	0.875	1.8825	0.9443	1.0937
	1.000	1.9437	0.9564	1.3127

Table 1.- Continued.

$a/c = 0.2$; $a/t = 0.8$; $h/b > 5$

$K/[S_i(\pi a/Q)^{1/2}]$

c/b	$2\phi/\pi$	TENSION	BENDING ABOUT X	BENDING ABOUT Z
	0.000	1.1608	0.7965	1.0949
	0.125	1.1641	0.7184	1.0979
	0.25	1.2867	0.6810	1.2160
	0.375	1.4379	0.6452	1.3646
0.04	0.50	1.5896	0.5892	1.5176
	0.625	1.7151	0.5198	1.6495
	0.75	1.8243	0.4478	1.7688
	0.875	1.9404	0.4083	1.8971
	1.000	2.0645	0.4142	2.0289
	0.000	1.1909	0.8101	1.0206
	0.125	1.1923	0.7294	1.0217
	0.25	1.3154	0.6928	1.1330
	0.375	1.4675	0.6576	1.2777
0.1	0.50	1.6198	0.6021	1.4324
	0.625	1.7453	0.5328	1.5732
	0.75	1.8545	0.4610	1.7069
	0.875	1.9715	0.4219	1.8533
	1.000	2.0976	0.4283	1.9978
	0.000	1.2665	0.8490	0.9308
	0.125	1.2629	1.7529	0.9278
	0.25	1.3881	0.7910	1.0305
	0.375	1.5437	0.6889	1.1726
0.2	0.50	1.6994	0.6358	1.3344
	0.625	1.8278	0.5683	1.4943
	0.75	1.9401	0.4983	1.6563
	0.875	2.0628	0.4616	1.8386
	1.000	2.1962	0.4689	2.0100

	0.000	1.5776	0.9977	0.6471
	0.125	1.5547	0.9088	0.6310
	0.25	1.6871	0.8740	0.7076
	0.375	1.8629	0.8479	0.8448
0.5	0.50	2.0458	0.8048	1.0361
	0.625	2.2079	0.7502	1.2673
	0.75	2.3632	0.6978	1.5340
	0.875	2.5503	0.6899	1.8504
	1.000	2.7494	0.7301	2.1239
	0.000	2.0587	1.2570	0.2744
	0.125	1.9773	1.1353	0.2393
	0.25	2.0948	1.0898	0.2809
	0.375	2.2857	1.0660	0.4105
0.8	0.50	2.5048	1.0345	0.6352
	0.625	2.7242	1.0008	0.9474
	0.75	2.9643	0.9829	1.3342
	0.875	3.2879	1.0341	1.8066
	1.000	3.6232	1.1347	2.2001

Table 1.- Continued.

$a/c = 0.4$; $a/t = 0.2$; $h/b > 5$

$K/[S_i(\pi a/Q)^{1/2}]$

c/b	$2\phi/\pi$	TENSION	BENDING ABOUT X	BENDING ABOUT Z
	0.000	0.7851	0.7278	0.7314
	0.125	0.7819	0.7031	0.7293
	0.25	0.8244	0.7108	0.7717
	0.375	0.8924	0.7387	0.8403
0.04	0.50	0.9620	0.7665	0.9128
	0.625	1.0240	0.7894	0.9806
	0.75	1.0760	0.8082	1.0408
	0.875	1.1184	0.8237	1.0928
	1.000	1.1316	0.8120	1.1132
	0.000	0.7883	0.7733	0.6572
	0.125	0.7846	0.7014	0.6581
	0.25	0.8272	0.7081	0.7008
	0.375	0.8954	0.7378	0.7707
0.1	0.50	0.9652	0.7675	0.8484
	0.625	1.0274	0.7912	0.9255
	0.75	1.0797	0.8105	0.9985
	0.875	1.1222	0.8224	1.0656
	1.000	1.1354	0.8022	1.0975
	0.000	0.7949	0.7374	0.5388
	0.125	0.7915	0.7186	0.5412
	0.25	0.8345	0.7269	0.5843
	0.375	0.9034	0.7556	0.6570
0.2	0.50	0.9739	0.7845	0.7435
	0.625	1.0370	0.8086	0.8365
	0.75	1.0901	0.8288	0.9313
	0.875	1.1335	0.8463	1.0236
	1.000	1.1473	0.8461	1.0736

Table 1.- Continued.

$a/c = 0.4$; $a/t = 0.5$; $h/b > 5$

$K/[S_i(\pi a/Q)^{1/2}]$

c/b	$2\phi/\pi$	TENSION	BENDING ABOUT X	BENDING ABOUT Z
	0.000	0.9498	0.7602	0.8919
	0.125	0.9342	0.6989	0.8779
	0.25	0.9705	0.6536	0.9144
	0.375	1.0389	0.6265	0.9836
0.04	0.50	1.1115	0.5990	1.0594
	0.625	1.1803	0.5721	1.1342
	0.75	1.2430	0.5520	1.2051
	0.875	1.3010	0.5421	1.2725
	1.000	1.3250	0.5296	1.3036
	0.000	0.9622	0.7692	0.8148
	0.125	0.9460	0.7006	0.8030
	0.25	0.9820	0.6555	0.8397
	0.375	1.0508	0.6290	0.9101
0.1	0.50	1.1237	0.6022	0.9907
	0.625	1.1928	0.5758	1.0743
	0.75	1.2560	0.5562	1.1574
	0.875	1.3145	0.5460	1.2392
	1.000	1.3388	0.5284	1.2809
	0.000	0.9908	0.7794	0.7030
	0.125	0.9734	0.7235	0.6935
	0.25	1.0096	0.6783	0.7312
	0.375	1.0794	0.6517	0.8051
0.2	0.50	1.1539	0.6252	0.8955
	0.625	1.2251	0.5995	0.9958
	0.75	1.2905	0.5811	1.1016
	0.875	1.3517	0.5737	1.2096
	1.000	1.3775	0.5621	1.2700

	0.000	1.1060	0.8717	0.3559
	0.125	1.0822	0.8063	0.3544
	0.25	1.1178	0.7593	0.3944
	0.375	1.1940	0.7358	0.4790
0.5	0.50	1.2792	0.7148	0.6005
	0.625	1.3654	0.6975	0.7546
	0.75	1.4505	0.6907	0.9337
	0.875	1.5358	0.6977	1.1280
	1.000	1.5770	0.6942	1.2514
	0.000	1.3102	1.0138	-0.0285
	0.125	1.2625	0.9315	-0.0243
	0.25	1.2830	0.8736	0.0155
	0.375	1.3587	0.8484	0.1094
0.8	0.50	1.4524	0.8312	0.2620
	0.625	1.5562	0.8234	0.4707
	0.75	1.6698	0.8330	0.7251
	0.875	1.7950	0.8638	1.0093
	1.000	1.8647	0.8769	1.1995

Table 1.- Continued.

$a/c = 0.4$; $a/t = 0.8$; $h/b > 5$

$K/[S_i(\pi a/Q)^{1/2}]$

c/b	$2\phi/\pi$	TENSION	BENDING ABOUT X	BENDING ABOUT Z
	0.000	1.2761	0.8446	1.2072
	0.125	1.2195	0.7334	1.1540
	0.25	1.2182	0.6179	1.1545
	0.375	1.2507	0.5157	1.1895
0.04	0.50	1.3100	0.4134	1.2527
	0.625	1.3718	0.3206	1.3211
	0.75	1.4498	0.2416	1.4071
	0.875	1.5546	0.1989	1.5209
	1.000	1.6630	0.1929	1.6348
	0.000	1.3085	0.8613	1.1373
	0.125	1.2491	0.7430	1.0863
	0.25	1.2457	0.6270	1.0878
	0.375	1.2769	0.5250	1.1253
0.1	0.50	1.3355	0.4228	1.1937
	0.625	1.3968	0.3303	1.2716
	0.75	1.4750	0.2516	1.3699
	0.875	1.5811	0.2092	1.4985
	1.000	1.6914	0.2017	1.6228
	0.000	1.3899	0.8848	1.0343
	0.125	1.3242	0.7767	0.9856
	0.25	1.3165	0.6589	0.9882
	0.375	1.3459	0.5556	1.0304
0.2	0.50	1.4046	0.4532	1.1082
	0.625	1.4675	0.3613	1.2033
	0.75	1.5492	0.2843	1.3243
	0.875	1.6622	0.2460	1.4806
	1.000	1.7802	0.2466	1.6247

	0.000	1.7588	1.0780	0.7581
	0.125	1.6592	0.9472	0.7130
	0.25	1.6301	0.8159	0.7176
	0.375	1.6558	0.7076	0.7775
0.5	0.50	1.7263	0.6070	0.8930
	0.625	1.8169	0.5247	1.0560
	0.75	1.9448	0.4662	1.2676
	0.875	2.1307	0.4588	1.5388
	1.000	2.3175	0.4880	1.7700
	0.000	2.4137	1.4182	0.4104
	0.125	2.2173	1.2370	0.3603
	0.25	2.1096	1.0630	0.3584
	0.375	2.1053	0.9345	0.4359
0.8	0.50	2.1843	0.8312	0.5948
	0.625	2.3269	0.7663	0.8388
	0.75	2.5512	0.7463	1.1595
	0.875	2.8995	0.8080	1.5728
	1.000	3.2390	0.9032	1.9134

Table 1.- Continued.

$a/c = 2.0$; $a/t = 0.2$; $h/b > 5$

$K/[S_i(\pi a/Q)^{1/2}]$

c/b	$2\phi/\pi$	TENSION	BENDING ABOUT X	BENDING ABOUT Z
	0.000	0.8006	0.7361	0.7576
	0.125	0.7881	0.7009	0.7471
	0.25	0.7568	0.6377	0.7195
	0.375	0.7224	0.5752	0.6896
0.04	0.50	0.6832	0.5156	0.6559
	0.625	0.6406	0.4612	0.6192
	0.75	0.6011	0.4173	0.5855
	0.875	0.5799	0.3938	0.5692
	1.000	0.5860	0.3975	0.5778
	0.000	0.8058	0.7374	0.6831
	0.125	0.7933	0.7011	0.6766
	0.25	0.7618	0.6376	0.6552
	0.375	0.7271	0.5753	0.6328
0.1	0.50	0.6877	0.5157	0.6080
	0.625	0.6448	0.4615	0.5806
	0.75	0.6050	0.4177	0.5558
	0.875	0.5839	0.3939	0.5473
	1.000	0.5900	0.3946	0.5607

Table 1.- Continued.

$a/c = 2.0$; $a/t = 0.5$; $h/b > 5$

$K/[S_i(\pi a/Q)^{1/2}]$

c/b	$2\phi/\pi$	TENSION	BENDING ABOUT X	BENDING ABOUT Z
	0.000	0.8244	0.6678	0.7806
	0.125	0.8092	0.5965	0.7676
	0.25	0.7742	0.4836	0.7362
	0.375	0.7367	0.3783	0.7034
0.04	0.50	0.6952	0.2871	0.6675
	0.625	0.6510	0.2145	0.6293
	0.75	0.6105	0.1635	0.5945
	0.875	0.5890	0.1359	0.5779
	1.000	0.5950	0.1338	0.5864
	0.000	0.8374	0.6844	0.7274
	0.125	0.8217	0.6101	0.7175
	0.25	0.7858	0.4951	0.6911
	0.375	0.7474	0.3885	0.6645
0.1	0.50	0.7051	0.2957	0.6362
	0.625	0.6601	0.2224	0.6062
	0.75	0.6190	0.1705	0.5795
	0.875	0.5973	0.1418	0.5701
	1.000	0.6036	0.1344	0.5833
	0.000	0.8746	0.7102	0.6475
	0.125	0.8577	0.6347	0.6403
	0.25	0.8192	0.5176	0.6216
	0.375	0.7785	0.4090	0.6049
0.2	0.50	0.7342	0.3147	0.5889
	0.625	0.6876	0.2396	0.5725
	0.75	0.6453	0.1867	0.5593
	0.875	0.6235	0.1578	0.5623
	1.000	0.6308	0.1505	0.5829

Table 1.- Continued.

$a/c = 2.0$; $a/t = 0.8$; $h/b > 5$

$K/[S_i(\pi a/Q)^{1/2}]$

c/b	$2\phi/\pi$	TENSION	BENDING ABOUT X	BENDING ABOUT Z
	0.000	0.8636	0.6118	0.8142
	0.125	0.8417	0.4994	0.7949
	0.25	0.7998	0.3376	0.7573
	0.375	0.7588	0.1919	0.7213
0.04	0.50	0.7170	0.0702	0.6851
	0.625	0.6769	-0.0213	0.6500
	0.75	0.6421	-0.0812	0.6218
	0.875	0.6305	-0.1143	0.6151
	1.000	0.6460	-0.1331	0.6333
	0.000	0.8864	0.6250	0.7748
	0.125	0.8632	0.5143	0.7578
	0.25	0.8193	0.3503	0.7240
	0.375	0.7764	0.2016	0.6930
0.1	0.50	0.7329	0.0774	0.6633
	0.625	0.6905	-0.0162	0.6353
	0.75	0.6557	-0.0775	0.6143
	0.875	0.6440	-0.1103	0.6145
	1.000	0.6599	-0.1215	0.6373
	0.000	0.9507	0.6577	0.7182
	0.125	0.9243	0.5442	0.7046
	0.25	0.8750	0.3763	0.6764
	0.375	0.8275	0.2243	0.6534
0.2	0.50	0.7803	0.0972	0.6342
	0.625	0.7351	0.0014	0.6181
	0.75	0.6988	-0.0613	0.6095
	0.875	0.6878	-0.0946	0.6221
	1.000	0.7062	-0.1064	0.6538

	0.000	1.3239	0.8358	0.6132
	0.125	1.2694	0.7059	0.6008
	0.25	1.1797	0.5146	0.5787
	0.375	1.1043	0.3449	0.5749
0.5	0.50	1.0411	0.2058	0.5874
	0.625	0.9906	0.1036	0.6118
	0.75	0.9605	0.0402	0.6486
	0.875	0.9726	0.0141	0.7117
	1.000	1.0212	0.0128	0.7827

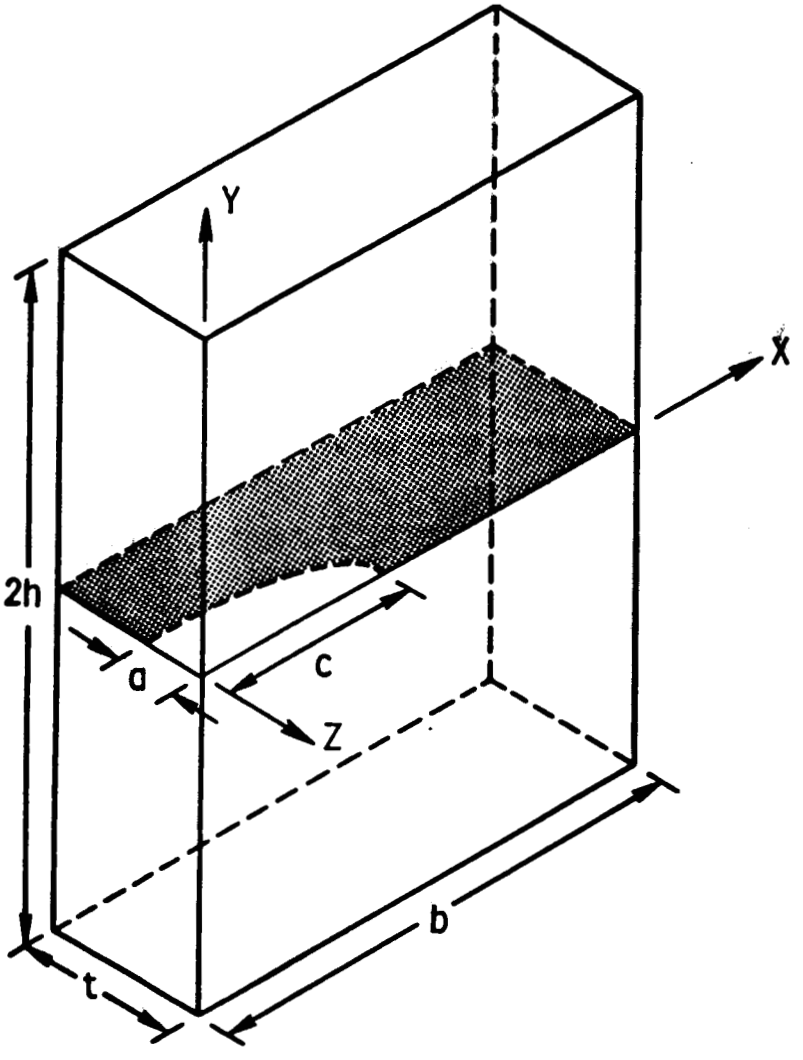

Fig. 1. - Quarter-elliptical corner crack in rectangular bar.

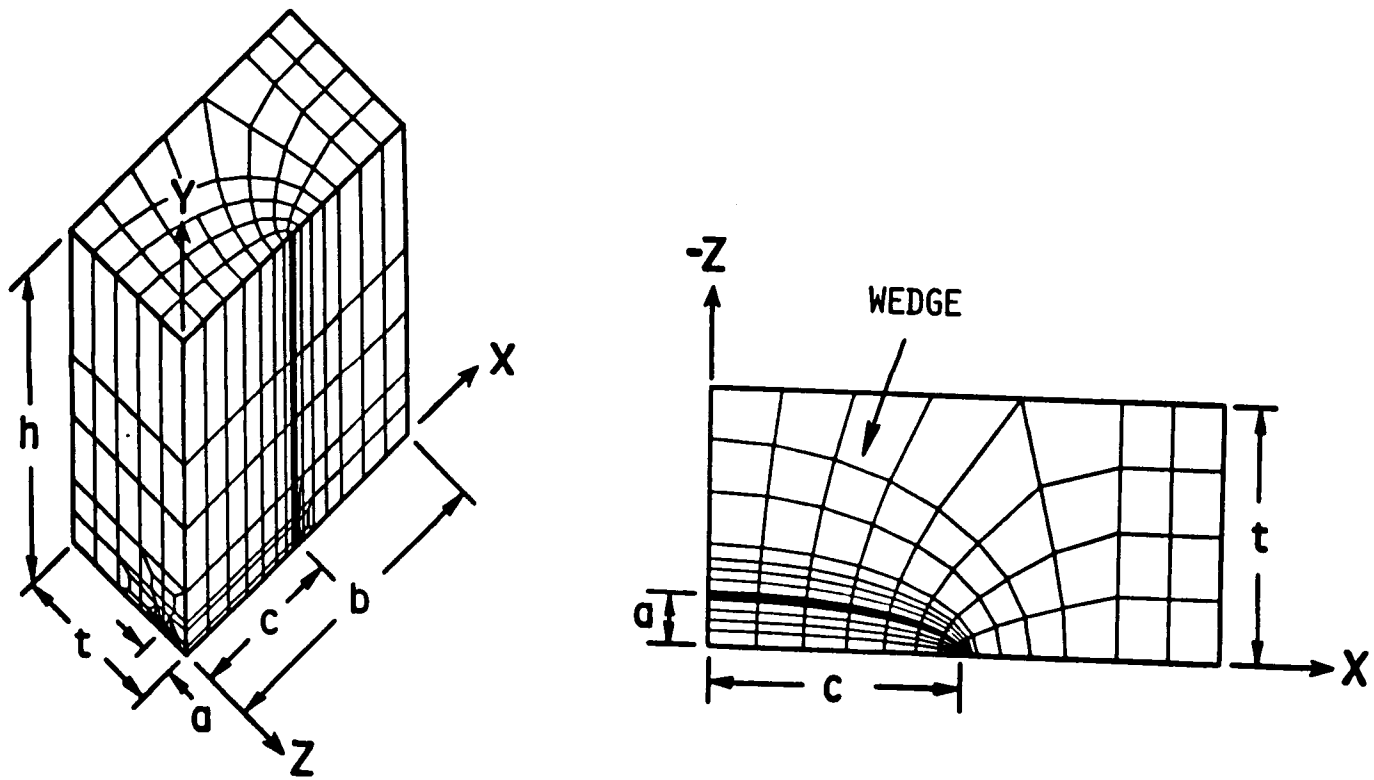

(a) Model of cracked bar.

(b) Mesh pattern on Y = 0 plane.

Fig. 2. - Finite-element mesh for surface and corner crack.

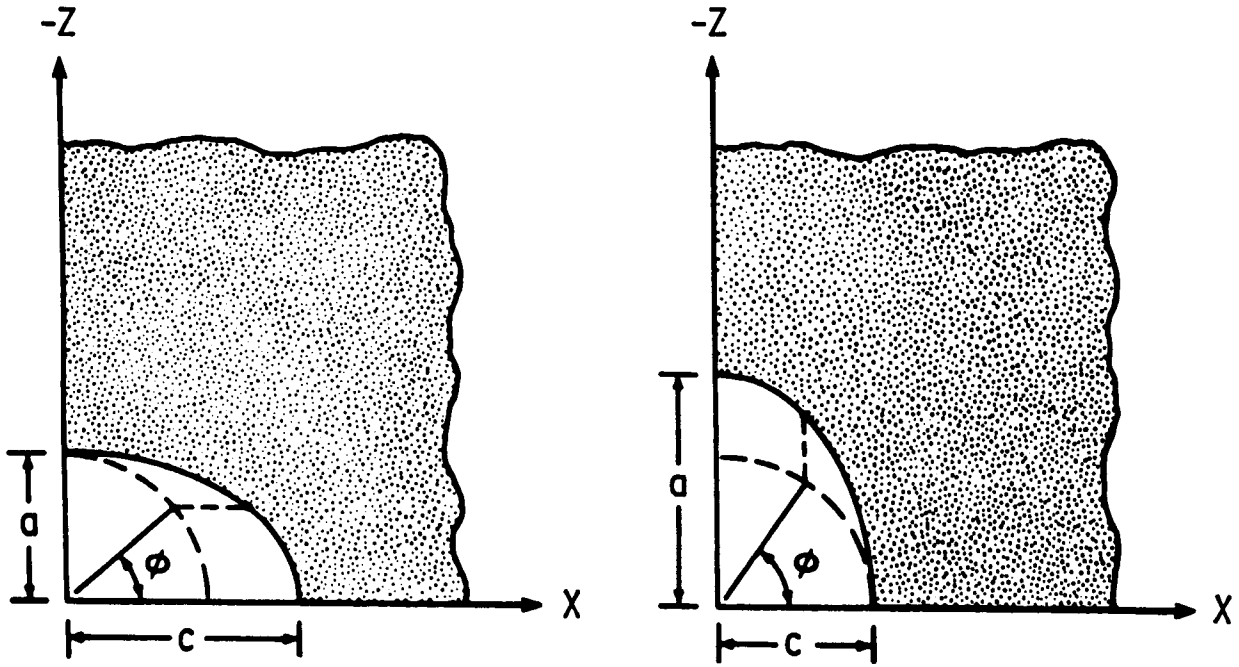

Fig. 3. - Definition of parametric angle.

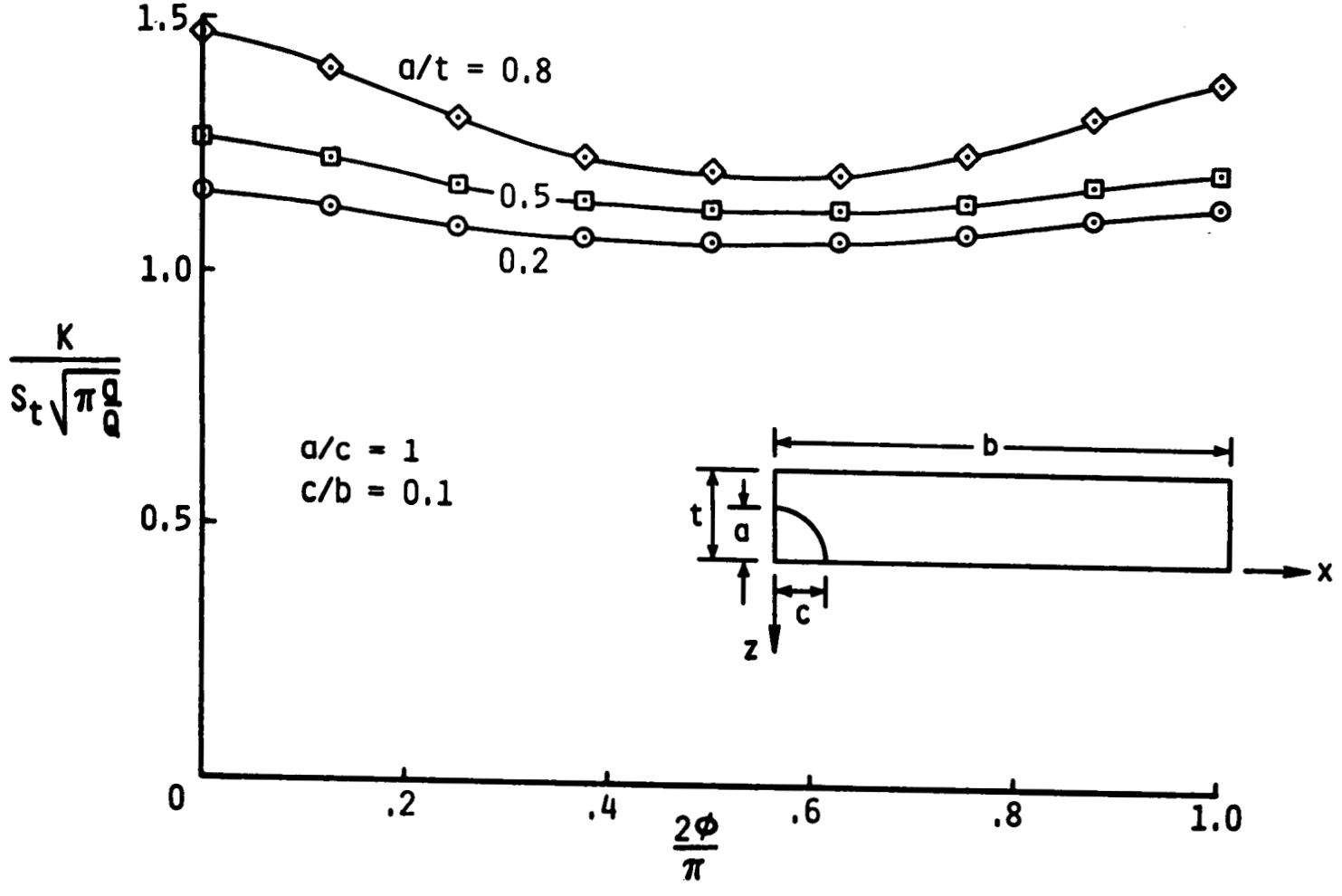

Fig. 4. - Normalized stress-intensity factors for a quarter-circular corner crack subjected to remote tension.

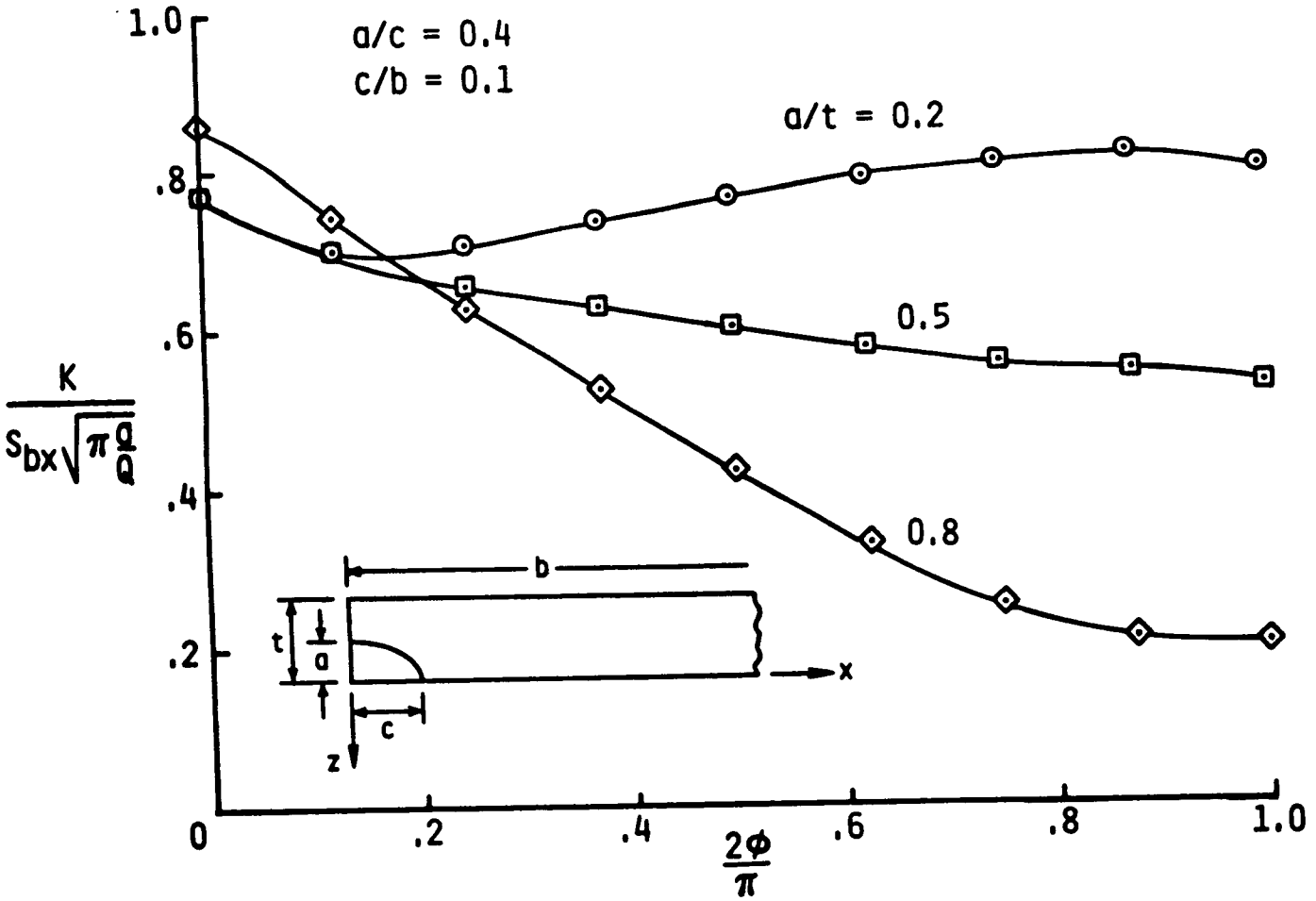

Fig. 5. - Normalized stress-intensity factors for a quarter-elliptic corner crack subjected to out-of-plane bending.

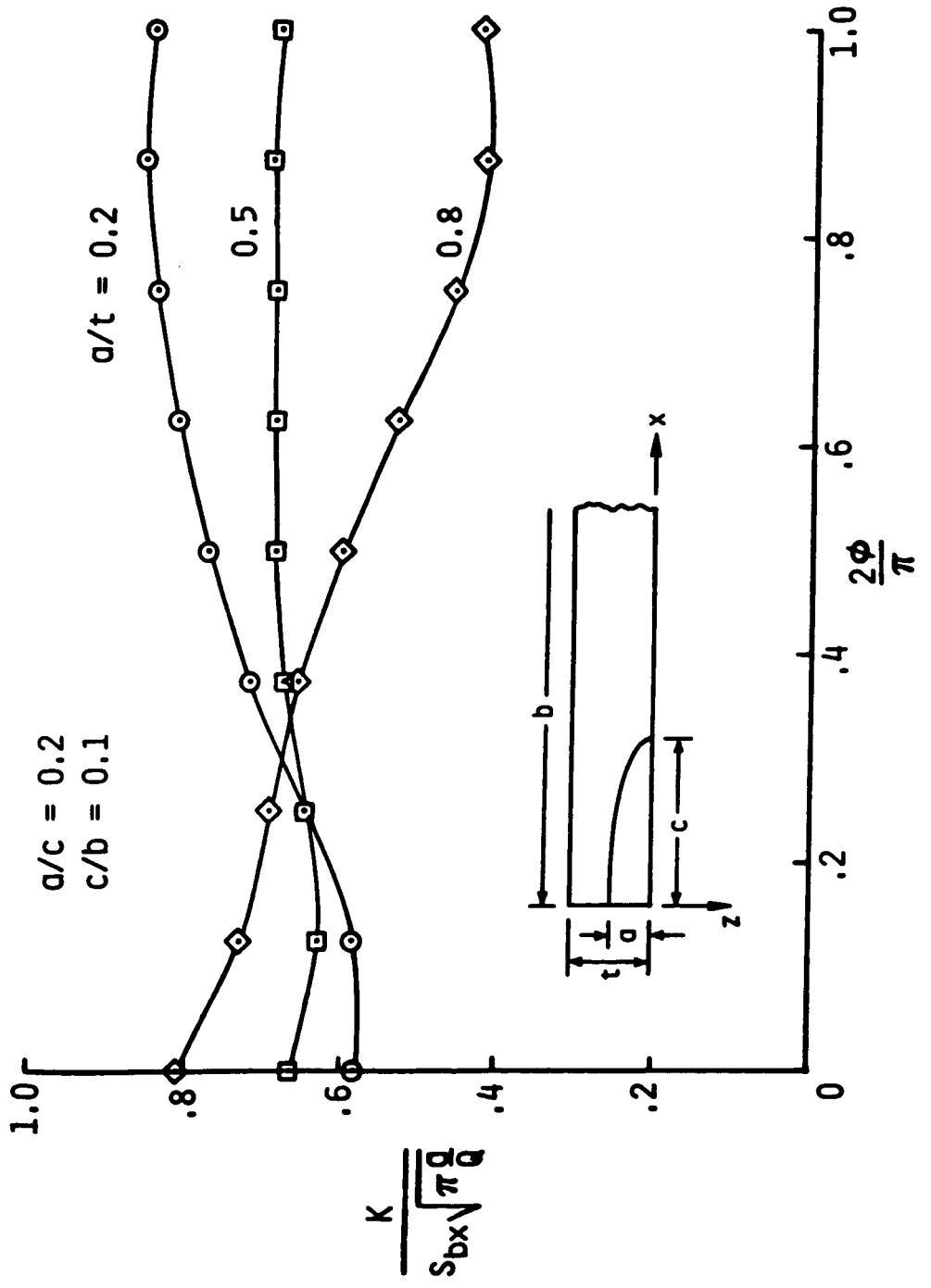

Fig. 6. - Normalized stress-intensity factors for a long quarter elliptic corner crack subjected to out-of-plane bending.

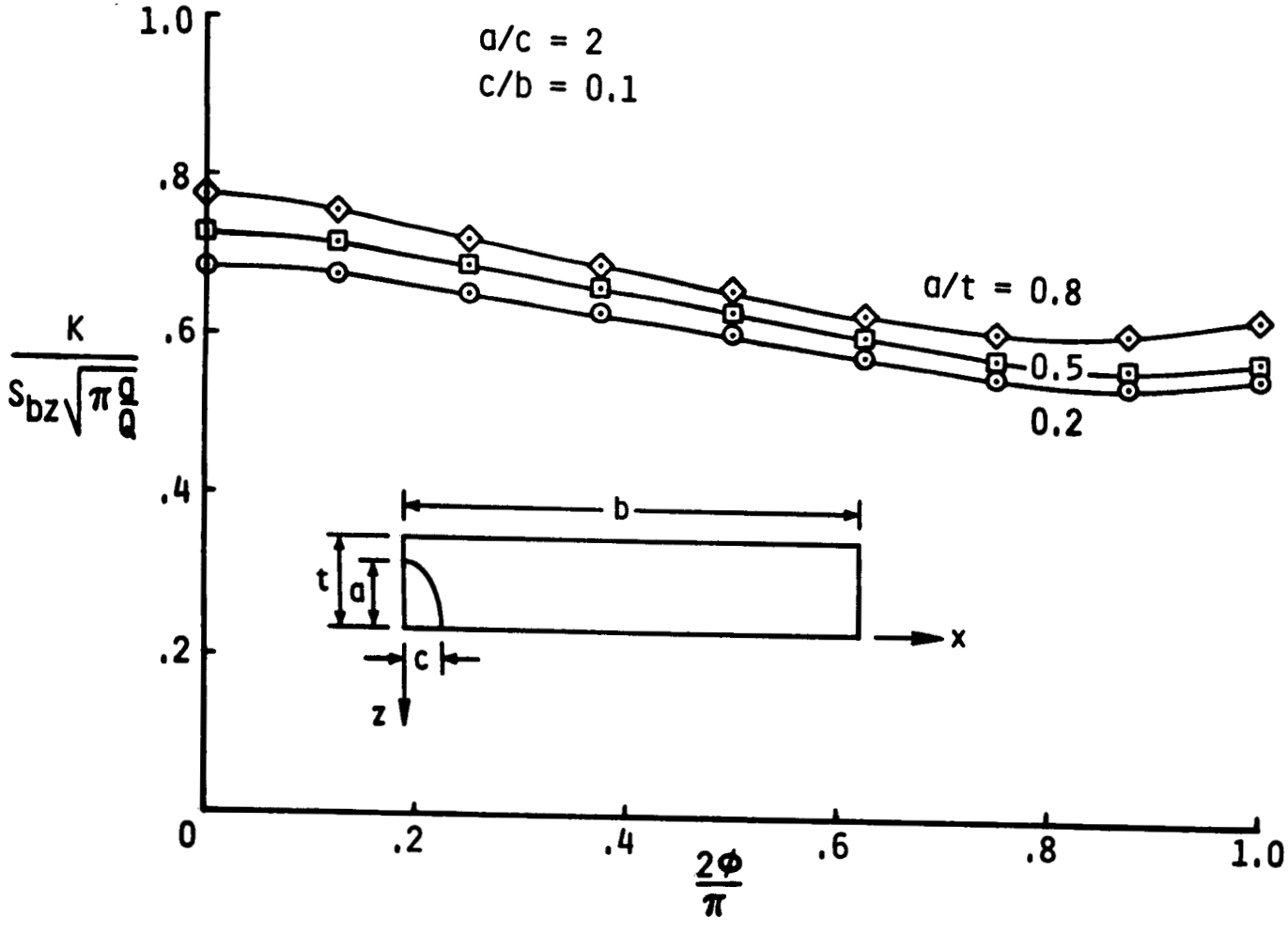

Fig. 7. - Normalized stress-intensity factors for a quarter-elliptic corner crack subjected to in-plane bending.

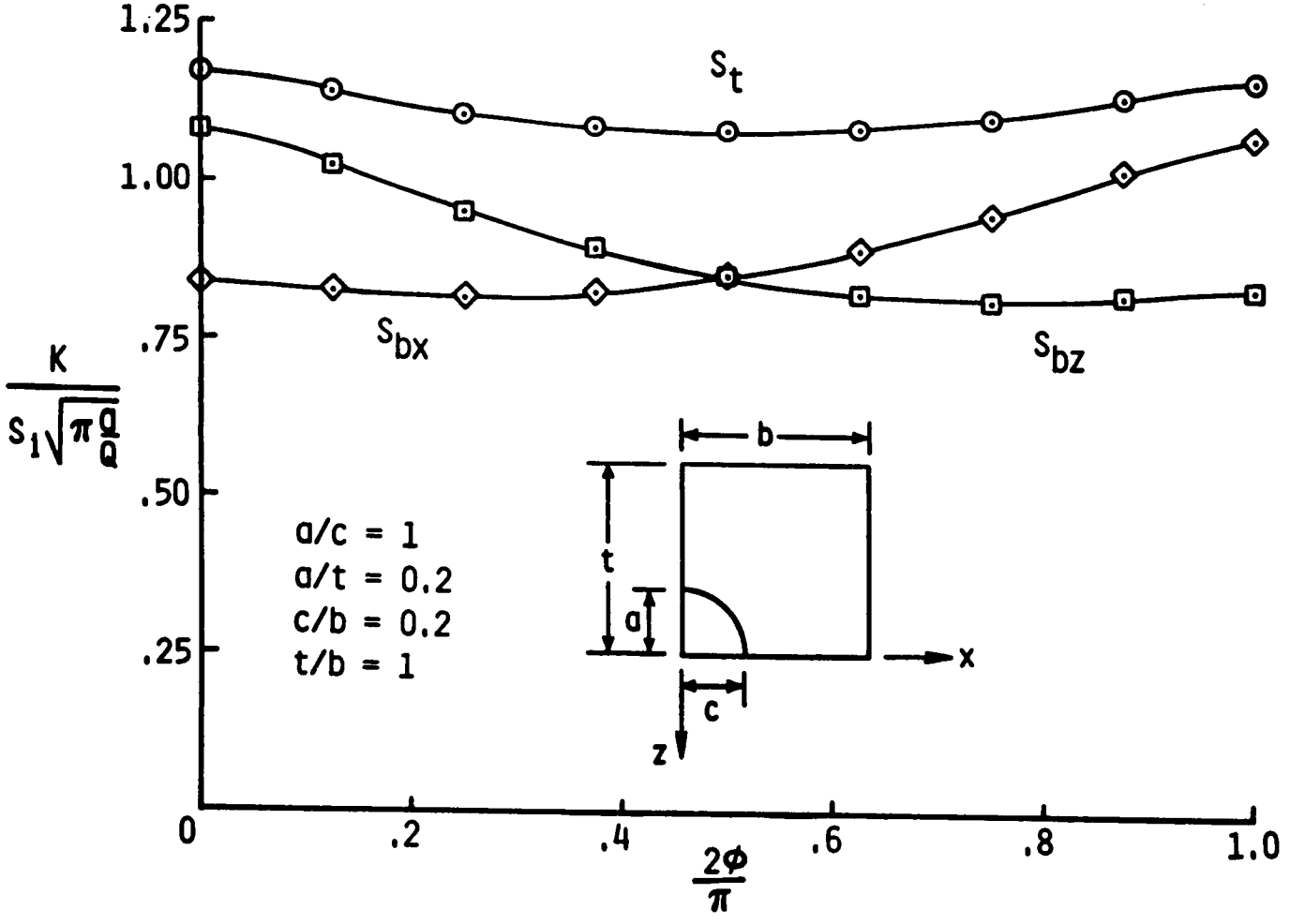

Fig. 8. - Normalized stress-intensity factors for a quarter-circular corner crack in a square bar subjected to various loading.

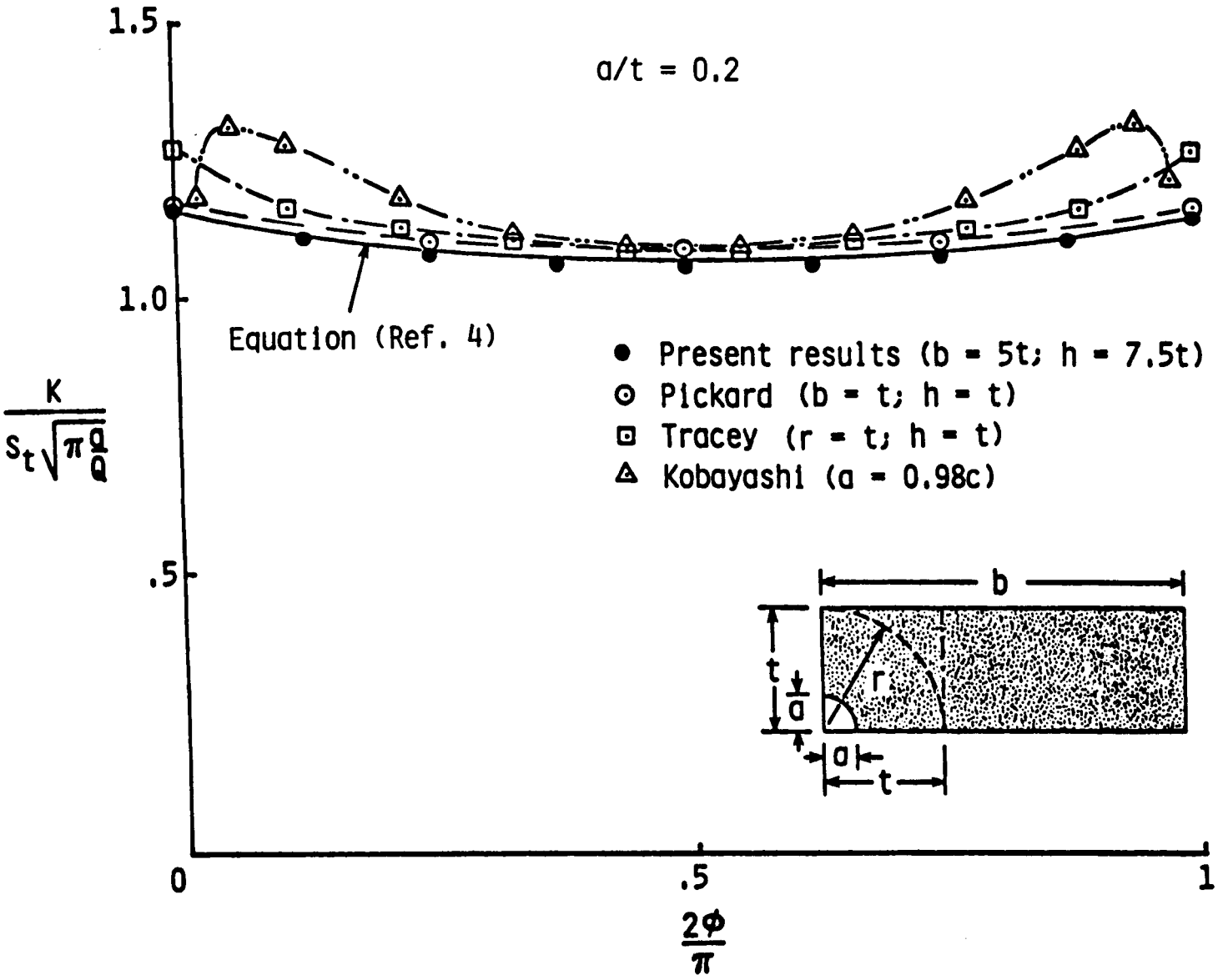

Fig. 9. - Comparison of normalized stress-intensity factors for quarter-circular corner crack subjected to remote tension.

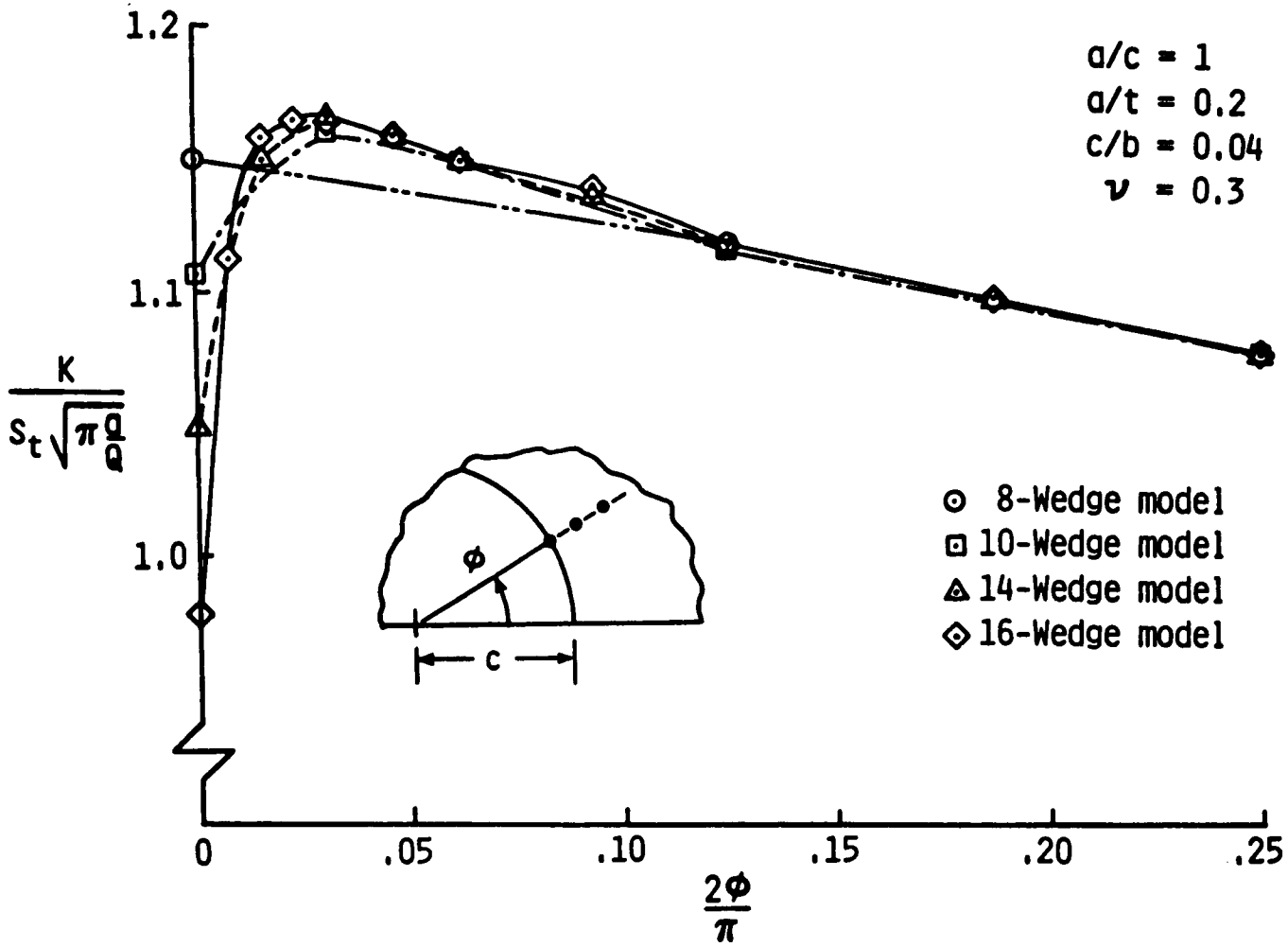

Fig. 10. - Effect of mesh refinement on normalized stress-intensity factors near a free surface.

Standard Bibliographic Page

1. Report No.	2. Government Accession No.	3. Recipient's Catalog No.
NASA TM-89070		

4. Title and Subtitle	5. Report Date
FINITE-ELEMENT ANALYSIS OF CORNER CRACKS IN RECTANGULAR BARS	June 1987
	6. Performing Organization Code
7. Author(s)	8. Performing Organization Report No.
I. S. Raju and J. C. Newman, Jr.	
9. Performing Organization Name and Address	10. Work Unit No.
NASA Langley Research Center Hampton, VA 23665-5225	506-43-11-04
	11. Contract or Grant No.
12. Sponsoring Agency Name and Address	13. Type of Report and Period Covered
National Aeronautics and Space Administration Washington, DC 20546	Technical Memorandum
	14. Sponsoring Agency Code

15. Supplementary Notes

I. S. Raju, Analytical Services & Materials, Inc., Hampton, Virginia.
J. C. Newman, Jr., Langley Research Center, Hampton, Virginia.

16. Abstract

This paper presents stress-intensity factors for a wide range of quarter-elliptical corner cracks in rectangular bars. Cracked configurations were subjected to remote tension, in-plane bending, or out-of-plane bending. The ratio of crack depth to crack length ranged from 0.2 to 2; the ratio of crack depth to specimen thickness ranged from 0.2 to 0.8; and the ratio of crack length to specimen width ranged from 0.04 to 0.8. The configurations analyzed varied from a square bar to a very wide plate. These particular crack configurations were chosen to cover the range of shapes and sizes that have been observed to grow in experiments conducted on rectangular bars. The stress-intensity factors were calculated by a three-dimensional finite-element method. Finite-element models employed singularity elements along the crack front and linear-strain elements elsewhere. The models had about 7000 degrees of freedom. Stress-intensity factors were calculated using a nodal-force method.

The present results were compared with other numerical results for a quarter-circular corner crack configuration. The present results along the interior of the crack generally agreed within 3 percent with those from the literature. Some larger differences (3 to 13 percent) were observed near the intersection of the crack front and the free surfaces (in the boundary-layer region). Thus, analyses were also performed to study the effect of mesh refinement in the boundary-layer region and the influence of Poisson's ratio on the distribution of stress-intensity factors.

17. Key Words (Suggested by Authors(s))

Cracks
Surface cracks
Crack propagation
Fracture
Stress analysis
Fatigue (materials)
Stress-intensity factors
Finite-elements
Boundary-layer region

18. Distribution Statement

Unclassified - Unlimited

Subject Category 39

19. Security Classif.(of this report)	20. Security Classif.(of this page)	21. No. of Pages	22. Price
Unclassified	Unclassified	46	A03

For sale by the National Technical Information Service, Springfield, Virginia 22161